Mon. Not. R. Astron. Soc. **000**, 000–000 (0000) Printed 25 March 2002 (MN LATEX style file v1.4)

XMM-Newton observations of the asynchronous polar BY Cam ⋆

Gavin Ramsay and Mark Cropper
Mullard Space Science Lab, University College London, Holmbury St. Mary, Dorking, Surrey, RH5 6NT, UK

Received:

ABSTRACT

We report observations of the asynchronous polar BY Cam made using *XMM-Newton*. We find evidence for two accretion regions which have significantly different spectra. In both regions we find evidence for hard X-ray emission from the post-shock flow while we observe a distinct soft X-ray blackbody emission in only one. We detect two emission lines in the RGS detectors which we attribute to Nitrogen NVI and NVII: the first time that Nitrogen lines have been detected in an X-ray spectrum of a cataclysmic variable. In the time interval where we observe short timescale variability we find the hard X-ray light curve is correlated with the softest energies in the sense that the hard X-rays trail the soft X-rays and are anti-correlated. We suggest that there are a small number of dense blobs of material which impact the white dwarf without forming a shock and release an amount of optically thick material which obscures hard X-rays for a short duration.

Key words: Stars: binaries: eclipsing – Stars: magnetic field – Stars: novae, cataclysmic variables – Stars: individual: BY Cam – X-rays: stars

1 INTRODUCTION

Polars are close binaries in which the primary star (a white dwarf) accretes material from a red dwarf secondary star. The strength of the magnetic field of the white dwarf (B$\sim$10–200 MG) is sufficient to synchronize its spin period with that of the binary orbital period. The accretion flow is controlled over large distances by the white dwarf's magnetic field. In most of these systems the magnetic field is locked into a single orientation with respect to the secondary star.

There are, however, four polars which are known not to be exactly synchronous: the spin period of the white dwarf differs from the orbital period by a few percent. It is expected that these systems are only temporarily out of phase-lock (due to eg a nova explosion) and will regain synchronization within several hundred years (Schmidt & Stockman 1991). One of the brightest of these asynchronous polars is BY Cam. It is bright in X-rays and has an binary orbital period of 201.258 mins and a white dwarf with a spin period of 199.330 mins (Mason et al 1998). This results in a spin-orbit beat period of 14.5 days.

BY Cam has been observed with various X-ray telescopes. Indeed, it was discovered using the X-ray satellite *Uhuru* by Forman et al (1978). Since then it has been observed using *EXOSAT* (Shrader et al 1988), *Ginga* (Ishida et al 1991, Done & Magdziarz 1998), *ASCA* (Kallman et al 1996, Done & Magdziarz 1998), *ROSAT* (Ramsay et al 1994, Mason et al 1998) and *BBXRT* (Kallman et al 1993). These observations have shown a highly variable X-ray light curve.

This variability is best shown in the *Ginga* data which was taken over 3 days and showed a periodic modulation in the first half which disappeared in the second half and was thereafter dominated by strong flaring. This is consistent with X-ray observations of one other asynchronous polar RX J2115–58 which showed highly variable light curves (Ramsay et al 2000). This variability was interpreted as the accretion flow rotating around the magnetic field of the white dwarf and at certain instances the flow accretes onto the opposite hemisphere of the white dwarf resulting in a different shaped light curve.

The hard X-ray spectra of BY Cam has shown evidence for a multi-temperature nature and complex absorption (Done & Magdziarz 1998). Using *ROSAT* data, Ramsay et al (1994) found that BY Cam was the one system which did not show a soft/hard X-ray ratio which was correlated with magnetic field strength. In this paper we present X-ray and simultaneous optical/UV observations of BY Cam using *XMM-Newton*.

⋆ Based on observations obtained with XMM-Newton, an ESA science mission with instruments and contributions directly funded by ESA Member States and the USA (NASA).

Instrument	Mode	Filter	Duration
EPIC pn	small window	thin	5063 sec
EPIC MOS	small window	thin	5924 sec
EPIC RGS			6406 sec
OM	image/fast	UVW1	1500 sec
OM	image/fast	V	1500 sec
OM	image/fast	UVW2	2000 sec

Table 1. The observation details of the various instruments onboard *XMM-Newton*.

2 OBSERVATIONS

BY Cam was observed for a short duration using *XMM-Newton* on 26 August 2001. We show in Table 1 the observation details in the various instruments. The EPIC instruments (imaging detectors covering the energy range 0.1–10keV with moderate spectra resolution) were operated in small window mode so that the effects of pile-up would be minimised. The RGS detectors (high resolution spectrographs operating in the 0.3–2.0keV range: den Herder et al 2001) were configured in the standard spectroscopy mode. For the OM (an optical/UV 30cm telescope: Mason et al 2001), data in 2 UV filters were obtained (UVW1: peak effective area at 2900 Å and bandwidth 750 Å UVW2: 2120 Å 450 Å) and one visual band (roughly the V band, 5500 Å 350 Å).

The data were processed using the *XMM-Newton Science Analysis Software* (SAS) v5.2. For the EPIC pn detector (Strüder et al 2001), data were extracted using an aperture of 40$''$ arc sec centered on the source. Background data were extracted from a source free region of the same CCD. For the EPIC MOS detectors (Turner et al 2001) we extracted the background from source free regions of other CCDs which were in full frame mode. The background data were scaled and subtracted from the source data. The OM data were analysed in a similar way using `omfchain` (using the version due to be released as part of the SAS v5.3). Data were corrected for background subtraction and coincidence losses (Mason et al 2001). Background subtracted RGS spectra were derived using the SAS tool `rgsproc`.

In extracting the EPIC pn spectra, we used only single pixel events and used the response file epn_sw20_sY9_thin.rmf. In the case of the MOS data we used the response files m[1-2]_thin1v9q19t5r5_all_15.rsp.

3 LIGHT CURVES

3.1 General Features

We show in Figure 1 the X-ray and optical/UV light curves. We are not able to phase the data on a spin or orbital ephemeris because of the uncertainty in the precise degree of asynchronism in this system. The light curves show that the X-ray observations commenced when the source was relatively faint (and showed a low soft/hard ratio). The source then increased in intensity and showed a significant amount of flaring activity towards the end of the observation (especially in the soft X-ray band) and showed an increased soft/hard ratio. The increase in X-ray flux is probably as a result of a second accretion region on the white dwarf rotating into view. Based on the flux levels found in §4.2, BY Cam was fainter by a factor of 5 and 3 compared to when it was observed using *ASCA* and *Ginga* but comparable to its *RXTE* observation. Although these comparisons are complicated by the fact that the *XMM-Newton* observations cover less than half of the binary orbital period, they do suggest that BY Cam was in a relatively high rather than a low accretion state when observed using *XMM-Newton*.

The UVW1 data shows a high count rate when the X-ray flux was low: the count rate (14.3 ct/s) corresponds to flux of $\sim 6.4\times10^{-15}$ ergs s^{-1} cm^{-2}Å (based on OM observations of isolated white dwarfs). The mean V band magnitude is ∼15.7 ($\sim 1.9\times10^{-15}$ ergs s^{-1} cm^{-2}Å), reaching a peak of ∼15.5. Since the V band data covered the period when the source was increasing in X-ray brightness it is likely that peak optical brightness in that orbital cycle was brighter than V ∼15.5. Silber et al (1997) present an extensive series of optical data on BY Cam. These show that when BY Cam is in a high state it can show a considerable variation in optical brightness, although typically around V ∼15 mag. Although the count rate in the UVW2 filter is low (1.9 ct/s) it corresponds to a flux of $\sim 7.5\times10^{-15}$ ergs s^{-1} cm^{-2}Å.

3.2 Short timescale variability

The first half of the X-ray light curves are relatively stable showing only small scale variability, mainly in the 1–10keV energy band (cf Figure 1). Around day 1.025, flaring activity starts to become prominent – particularly at energies below 0.5keV. To study the nature of the short term flaring in greater detail we examined data in the time range starting from this point until the end of the observation.

We show in Figure 2 the auto-correlation function of the energy resolved light curves using the EPIC pn data. This shows that the zero-crossing time in the 0.3–0.5keV and 1–10keV light curves are both around ∼85 sec. However, in the softest band (0.1–0.3keV), this value is much longer taking around ∼300 sec. In comparison, observations of the polar EF Eri showed the zero-crossing time was ∼85 sec in *EXOSAT* (both in the CMA:0.04–2keV and ME: 2–6keV) observations (Watson, King & Williams 1987) and around ∼55 sec in both soft and hard bands of *ROSAT* data (Beuermann, Thomas & Pietsch 1991).

We also cross-correlated the EPIC pn 0.1–0.3keV and 1–10keV light curves (Figure 2). This shows that the peak of the cross correlation deviates from zero (25±15 sec) and is significantly greater than other peaks in the delay range –400 to +400 sec. This suggests that this correlation is significant and implies that the 1–10keV light curve *trails* the 0.1–0.3keV light curve and is *anti-correlated*. This means that when there is a brightening in the 0.1–0.3keV light curve there is a dip in the 1–10keV light curve shortly afterwards. We also repeated the same analysis using the EPIC MOS data and find the same result as for the EPIC pn data. This is an entirely unexpected result which is discussed further in §5.

We made a search for Quasi Periodic Oscillations (QPO) in the X-ray light curve. This was done by examining a number of different time intervals and energy bands. We found no evidence for a significant QPO signal (on timescales

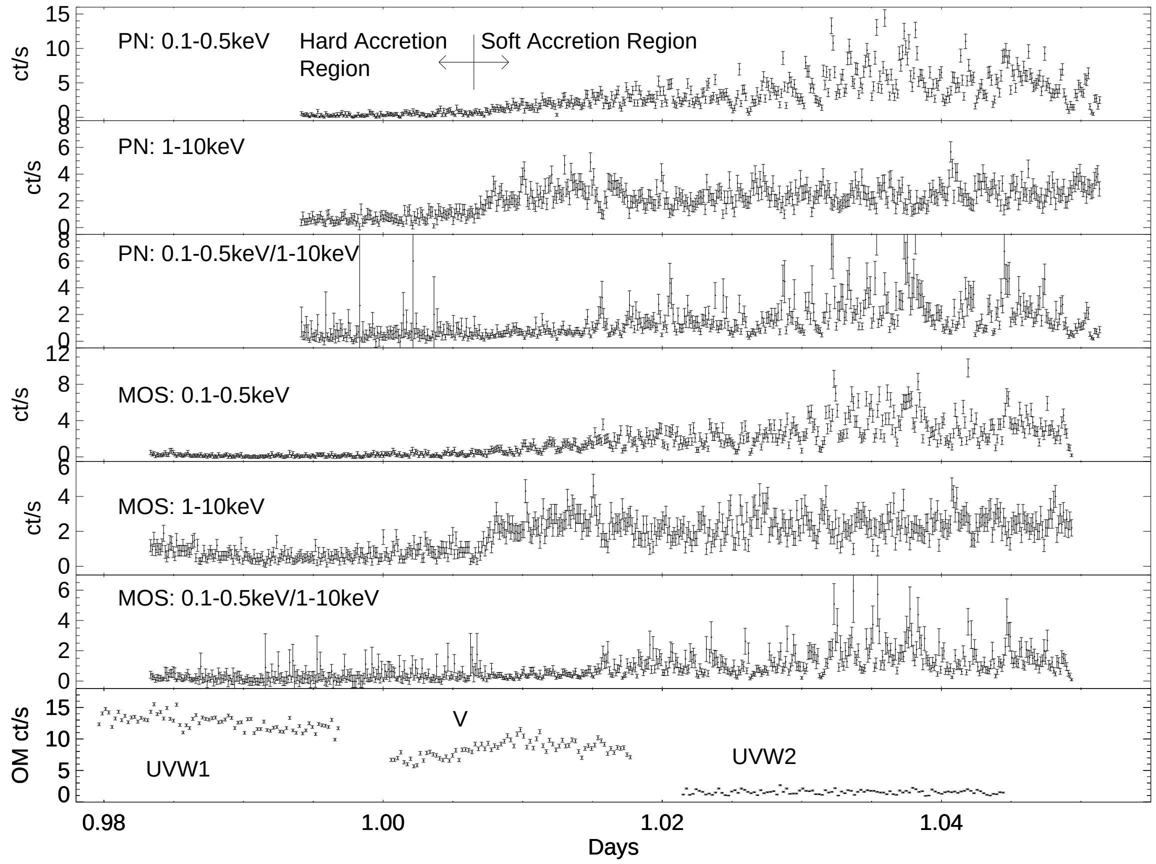

Figure 1. The X-ray and optical/UV light curves of BY Cam observed using *XMM-Newton*. The MOS 1 and 2 data have been co-added. The days are TDB-2452147.0 corrected for light travel time to the solar system barycentre. The 'hard' and 'soft' accretions denote time intervals in the text.

between 0.1 sec and 50sec) in the Discrete Fourier Transforms.

4 X-RAY SPECTRA

4.1 RGS spectra

Although the count rate in the RGS instruments was low (~0.2 ct/s), it was sufficient to extract a spectrum with sufficient signal-to-noise to search for prominent features. We show in Figure 3 the RGS1 and RGS2 spectra. There are two lines which are apparent in both instruments suggesting they are real instruments: at $0.427^{+0.011}_{-0.006}$keV and $0.500^{+0.002}_{-0.003}$ keV. They have equivalent widths of 8^{+21}_{-2}eV and 35^{+31}_{-15}eV respectively. They are probably due to NVI (0.4262 or 0.4307 keV) and NVII (0.500 keV).

4.2 EPIC spectra

The hardness ratios shown in Figure 1 suggest that the accretion region which is viewed at the beginning of the observation is harder than the second accretion region which come into view at day 1.007. We therefore extracted spectra from time intervals corresponding to the first visible accretion region (the 'hard' region) and the second visible region (the 'soft' region). Our emission model consisted of neutral absorbing material and a multi-temperature shock model (Cropper et al 1999). This model takes into account cooling via cyclotron radiation, a variation in the gravitational force over the height of the post-shock flow and the multi-temperature nature of this region: the immediate layers beneath the shock front reaches temperatures ~30-50keV, while closer to the white dwarf photosphere it has cooled to ~1keV. We fix the ratio of cyclotron to bremsstrahlung cooling, ϵ_s at 5, appropriate for the magnetic field strength of the white dwarf in BY Cam (thought to be in the range 30–50MG: Cropper et al 1989). When necessary we added a neutral absorption which had a partial covering fraction and a blackbody. We also added a Gaussian component to model the fluorescent line at 6.4keV. We fitted the spectra from the three EPIC detectors separately.

We show in the left hand panel of Figure 4 the EPIC pn spectrum covering the hard time interval. The spectral parameters for all three spectra are shown in Table 2. The immediate points to note are the absence of a soft blackbody component and the low column density. We define the hard X-ray luminosity as $L_{hard} = 4\pi \mathrm{Flux}_{hard,bol} d^2$ where $\mathrm{Flux}_{hard,bol}$ is the unabsorbed, bolometric flux from the hard component and d is the distance. Since a fraction of this flux is directed towards the observer, we switch the reflected component to zero after the final fit to determine the intrinsic flux from the optically thin post-shock region. For a distance of 100pc we find that $L_{hard} \sim 10^{31}$ ergs s^{-1}.

For the spectra covering the soft time interval we find that a soft blackbody component is required to achieve good

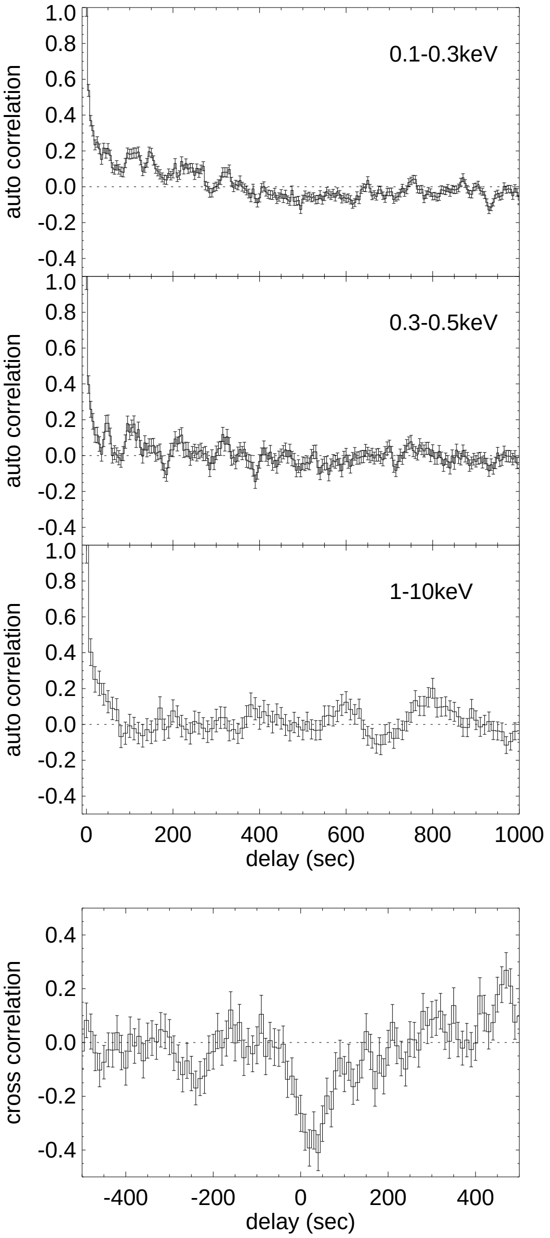

Figure 2. From the top: The autocorrelation for the EPIC pn light curve in the 0.1-0.3keV, 0.3–0.5keV and 1–10keV energy bands using data from day 1.025 until the end (cf Figure 1). The time bin is 5 sec in each case. Bottom panel: the cross correlation function of the 0.1–0.3keV and 1–10keV light curves. The positive time lag implies the hard X-ray light curve *trails* the soft X-ray light curve and is anti-correlated.

fits to the data. Further, in addition to the neutral absorption component we require a second absorption component with a partial covering fraction. We show the EPIC pn spectrum in the right hand panel of Figure 4 and the spectral parameters in Table 3. We define the soft X-ray luminosity as $L_{soft} = \pi \mathrm{Flux}_{soft,bol} \sec(i-\beta) d^2$, where we assume that the soft X-ray emission is optically thick and can be approximated by a small thin slab of material, the unabsorbed bolometric flux is $\mathrm{Flux}_{soft,bol}$, i the inclination and β the angle between the accretion region and the spin axis. Taking i ~40–60° and β ~100–125° (assuming the soft pole is negatively circularly polarised: Piirola et al 1994) we find $\sec(i-\beta)$ ~2. The ratio of L_{soft}/L_{hard} ~0.5. This is similar to that found by Ramsay et al (1994) using *ROSAT* data. They suggested that because BY Cam is an asynchronous system the accretion region may have a larger area than is typical in polars because the aspect of the white dwarf is continuously changing with respect to the accretion stream. Extracting a spectrum from the second half of the soft interval we find that the soft/hard flux increases by a factor of ~4: this is consistent with the view that the soft flaring is due to dense blobs of material which impact directly into the photosphere of the white dwarf without forming a shock.

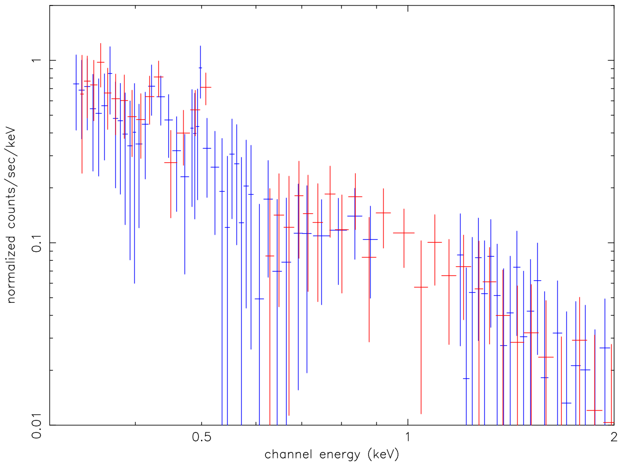

Figure 3. The integrated spectrum in the RGS 1 & 2 instruments. Although the signal to noise of the spectra are low, lines are seen at 0.426keV and 0.500keV in both instruments.

Our spectral fits also allow us to determine the mass of the white dwarf using the Nauenberg (1972) mass-radius relationship for white dwarfs. Tables 2 and 3 show that we find a mass 0.9–1.1$M_\odot$. This is consistent with the mass determined using *Ginga* data (0.98$M_\odot$: Cropper et al 1999) and *RXTE* data (1.04$M_\odot$: Ramsay 2000).

5 DISCUSSION

5.1 Short time variability

Various groups have searched for a correlation between the soft and hard X-ray light curves of polars. Observations of AM Her (Stella, Beuermann & Patterson 1986) showed no correlation between the soft and hard X-ray light curves while observations of EF Eri (Watson, King & Williams 1987) found that the soft and hard X-ray light curves were weakly correlated at zero lag. However, in both of these cases, the 'soft' X-ray light curve extended up to 2keV or beyond and hence their 'soft' band may have been contaminated by photons originating from the post-shock flow. With the good spectral resolution of *XMM-Newton* we have been able to separate the soft re-processed X-ray emission from the post-shock emission.

In §3.2 we found evidence that the hard X-ray light curve trailed the softest X-ray light curve by ~10–40sec and was anti-correlated. This is an unexpected result. The emission at energies 0.1–0.3keV is produced by a combination

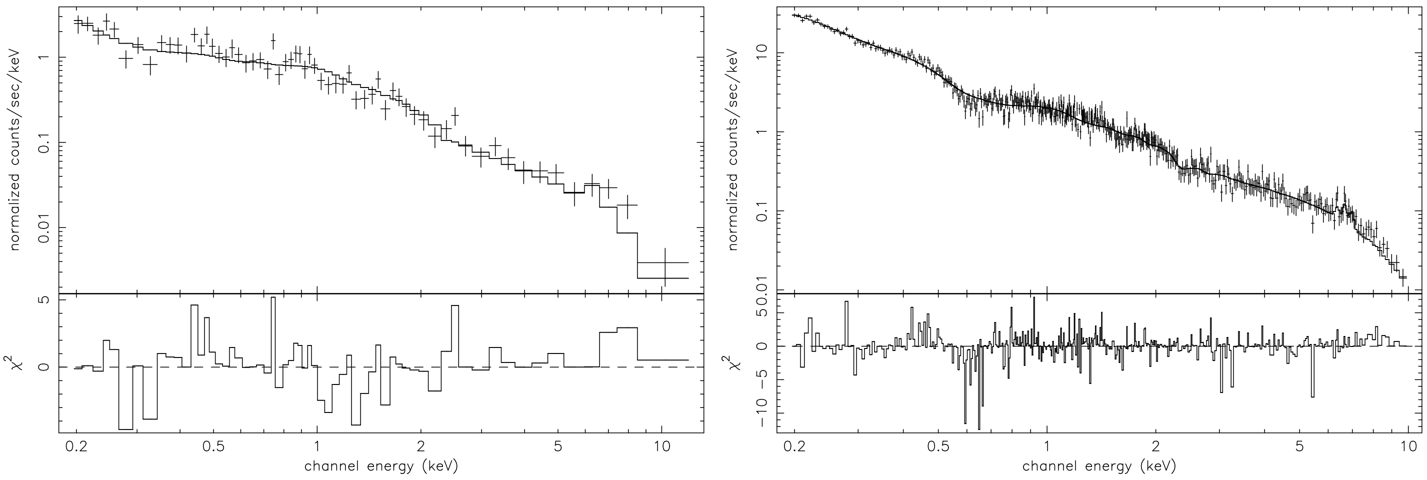

Figure 4. The EPIC pn spectra of the 'hard' (left hand panel) accretion region and the 'soft' accretion region (right hand panel). A soft X-ray component is only seen in the 'soft' accretion region.

Detector	N_H ($\times 10^{19}$ cm^{-2})	M_1 ($M_\odot$)	Observed flux (0.1–10keV) ergs s^{-1} cm^{-2}	Unabsorbed flux Bolometric ergs s^{-1} cm^{-2}	Shock flux Bolometric ergs s^{-1} cm^{-2}	χ^2_ν (dof)	L_X ergs s^{-1}
EPIC pn	0^{+4}	$0.9^{+0.2}_{-0.1}$	$6.1\pm0.5 \times 10^{-12}$	$1.0\pm0.1 \times 10^{-11}$	$9.7\pm0.9 \times 10^{-12}$	1.38 (57)	$1.2\pm0.1 \times 10^{31}$
EPIC MOS1	0^{+8}	$1.14^{+0.12}_{-0.17}$	$6.0\pm1.5 \times 10^{-12}$	$1.2\pm0.3 \times 10^{-11}$	$1.1\pm0.3 \times 10^{-11}$	1.34 (49)	$1.3\pm0.4 \times 10^{31}$
EPIC MOS2	0	$0.94^{+0.10}_{-0.16}$	$5.8^{+1.6}_{-0.6} \times 10^{-12}$	$1.0^{+0.3}_{-0.1} \times 10^{-11}$	$9.5^{+2.6}_{-1.0} \times 10^{-12}$	0.99 (92)	$1.1^{+0.4}_{-0.1} \times 10^{31}$

Table 2. The results of our spectral fits to the EPIC data covering the hard accretion region. The errors levels refer to the 90 percent confidence level. The shock flux refers to the flux originating solely from the post-shock flow and excluding the hard X-rays reflected from the white dwarf. We assume a distance of 100pc in determining the luminosities.

of hard X-rays irradiating the white dwarf and then being re-radiated at lower energies (Lamb & Masters 1979, King & Lasota 1979), and dense blobs of material penetrating the photosphere of the white dwarf (Kuijpers & Pringle 1982). The proportion of blobs present in the accretion flow is thought to be proportional to the magnetic field strength of the white dwarf (Ramsay et al 1994). At energies above $\sim$1keV the emission is due entirely from X-rays produced in the post-shock region above the photosphere of the white dwarf. If soft X-rays were produced largely from the reprocessing of hard X-rays then they would be expected to be correlated (it is possible there would be a short time delay with the soft band trailing the hard since it would take a finite time for the hard X-rays to be reprocessed). We suggest that the observed delayed anti-correlation is due to dense blobs of material impacting the photosphere of the white dwarf which then throw-up enough optically thick material to obscure even hard X-rays for a short time. Supporting evidence is found from the spectral fits which indicate the absorption is significantly higher in the soft accretion region spectrum compared to the hard accretion region spectrum.

5.2 Spectra

The RGS spectra show the presence of line emission at 0.426 and 0.500 keV. These lines appear to be due to NVI and NVII. We believe that this is the first time that Nitrogen lines have been seen in the X-ray spectra of a CV. This observation is interesting since Bonnet-Biduad & Mouchet (1987) using *IUE* spectra found that the ratio of NV/CIV is unusually large - around a factor of 20 greater than normally found in polars. They suggested that this unusual ratio was due to a previous nova event in the system. The lines detected in the X-ray band are of course more ionised that those seen in the UV but their origin (whether in the pre-shock accretion flow, circumbinary material or from the white dwarf photosphere), is still unclear.

Another significant result from our spectral fitting is the finding that no blackbody component is seen in the 'hard' accretion region while it is in the 'soft' accretion region. A soft X-ray component has been seen in many polars, but there are examples where none have been detected. The polar WW Hor was observed using *XMM-Newton* (Ramsay et al 2001) in an intermediate accretion state and no soft X-ray component was detected. Further, the soft and hard X-ray light curves are almost always seen in phase. However, there have been some observations where the soft and hard X-ray components have been seen in anti-phase (the 'reversed X-ray mode'). One example is the observation of AM Her made using *EXOSAT* (Heise et al 1985). This observation contrasts with other observations of AM Her which show the soft and hard light curves in phase.

Heise et al (1985) suggest that AM Her normally accretes only onto one magnetic pole, but in the reversed X-

Detector	N_H ($\times10^{20}$ cm^{-2})	N_H ($\times10^{20}$ cm^{-2})	cvf	kT_{bb} (eV)	Observed bb flux (0.1–10keV) (10^{-12} ergs s^{-1} cm^{-2})	Bolometric bb flux (10^{-11} ergs s^{-1} cm^{-2})	L_{soft} (10^{31} ergs s^{-1})
EPIC pn	2.7±0.5	7^{+9}_{-2}	$0.41^{+0.08}_{-0.06}$	54±3	$5.8^{+1.5}_{-1.4}$	3.9±1.0	2.3±0.6
EPIC MOS1	$2.0^{+4.0}_{-0.6}$	8^{+16}_{-1}	0.40±0.06	54^{+3}_{-6}	$6.2^{+4.6}_{-2.3}$	$5.3^{+2.4}_{-1.1}$	$3.2^{+1.5}_{-0.7}$
EPIC MOS2	$2.2^{+1.0}_{-0.8}$	17^{+8}_{-5}	$0.56^{+0.07}_{-0.08}$	52^{+3}_{-4}	7.7^{+6}_{-2}	$8.4^{+6.5}_{-2.1}$	$5.0^{+4.0}_{-3.8}$

Detector	M_1 ($M_{\odot}$)	Observed hard flux (0.1–10keV) (10^{-11} ergs s^{-1} cm^{-2})	Bolometric hard flux (10^{-11} ergs s^{-1} cm^{-2})	Shock Bolometric flux (10^{-11} ergs s^{-1} cm^{-2})	L_{hard} (10^{31} ergs s^{-1})	L_{soft}/L_{hard}	χ^2_ν (dof)
EPIC pn	$0.91^{+0.07}_{-0.06}$	$2.0^{+0.2}_{-0.1}$	$4.6^{+0.5}_{-0.2}$	$4.4^{+0.5}_{-0.2}$	$5.3^{+0.6}_{-0.3}$	$0.43^{+0.15}_{-0.14}$	1.07 (418)
EPIC MOS1	$1.10^{+0.05}_{-0.06}$	2.2±0.02	$6.1^{+0.5}_{-0.6}$	$5.7^{+0.5}_{-0.6}$	$6.9^{+0.6}_{-0.7}$	$0.46^{+0.3}_{-0.13}$	1.58 (124)
EPIC MOS2	$1.01^{+0.09}_{-0.18}$	$2.3^{+0.05}_{-0.3}$	$7.6^{+1.7}_{-1.0}$	$7.2^{+1.7}_{-1.0}$	$8.6^{+2.0}_{-1.2}$	$0.58^{+0.63}_{-0.47}$	1.15 (127)

Table 3. The fit parameters to the 'soft' accretion region. In the top panel we show the flux from the blackbody component and the hard X-ray component in the bottom. We assume a distance of 100pc in determining the luminosities.

ray mode, accretion occurs onto both poles. When accreting onto only one pole (the primary pole), both soft and hard X-rays are generated. When accretion occurs on the secondary pole, accretion takes place in the form of dense blobs of material which penetrate directly the white dwarf photosphere and no shock is formed: this pole is therefore strong in soft X-rays. Polarimetric observations of BY Cam by Piirola et al (1994) show evidence for positive and negative circular polarisation, implying the presence of two accretion poles.

Dealing with the 'soft' pole first, there is clear evidence of short term variations in the soft X-ray light curve (at least in the second half of the soft light curve). Since there are no short term variations in the hard X-ray light curve, the most probable mechanism for the soft flaring is dense blobs of material which impact directly into the white dwarf. This would be expected to reflected in a high L_{soft}/L_{hard} ratio. In contrast, the fits to the spectrum of the soft accretion region imply a ratio ~0.5 which is consistent with the 'standard' accretion model in which the soft X-ray emission originates entirely from re-processing of hard X-rays. However, when we consider the spectrum taken from the only the flaring state, we find that the soft/hard ratio increases by a factor of 4. This is consistent with the view that dense blobs of material are indeed present in the flow and are the cause of flaring in soft X-rays.

We now discuss the hard accretion region. Compared to the soft accretion region, the hard region shows a light curve which is much more constant in intensity. This suggests the absence of dense blobs of material impacting onto this accretion pole. However, we would still expect there to be a soft X-ray component from re-processing of the hard X-ray component. If the accretion rate was reduced (the hard X-ray flux is a factor ~5 lower in this region compared to the soft region) or the flow was spread over a larger area than usual, then the temperature of the re-processed component would be lower. This would result in the re-processed component being shifted into UV wavebands. Indeed, Figure 1 shows that the UVW1 count rate is high when the hard region is in view.

To investigate this further, we re-considered the soft accretion region spectrum by adding a blackbody of temperature 1.7eV (20000K, Gänsicke, Beuermann & de Martino 1998) to account for that part of the white dwarf not heated by the accretion flow. We then set the normalisation of this component to match the flux observed in the UVW2 filter. We then added this low temperature blackbody to our model for the hard accretion region. We find that the observed flux in the UVW1 filter is higher by a factor ~2 than predicted. We now add a second blackbody to account for a re-processed component: this is fixed at various temperatures and normalisations so that it gives the observed UVW1 flux and has no significant effect on the fit to the X-ray spectra.

We find that for a heated region of temperature ~4eV (as opposed to 54eV in the soft accretion region), we find L_{soft}/L_{hard} ~1. (Here we set sec$(i-\beta)$=1 appropriate for the positively circularly polarised pole which we take to be the hard accretion region, Piirola et al 1994). Some degree of caution should be applied there are uncertainties in the exact temperature of the unheated white dwarf, the precise UV flux estimates and the amount of absorption. However, this supports our view that the lack of a distinct soft X-ray component in the hard accretion region is because this component has moved into the UV as a result of the lower hard X-ray heating rate, or that it is spread over a larger area compared to the soft accretion pole. This is similar to that observed in AM Her (Gänsicke, Beuermann & de Martino 1998).

REFERENCES

Beuermann, K., Thomas, H.-C., Pietsch, W., 1991, A&A, 246, L36

Bonnet-Bidaud, J. M., Mouchet, M., 1987, A&A, 188, 89

Cropper, M., 1989, MNRAS, 236, 29P

Cropper, M., Ramsay, G., Wu, K., 1998, MNRAS, 293, 222

Cropper, M., Wu, K., Ramsay, G., Kocabiyik, A., 1999, MNRAS, 306, 684

den Herder, J. W., et al, 2001, A&A, 365, L7

Done, C., Magdziarz, P., 1998, MNRAS, 298, 737

Gänsicke, B., Beuermann, K., de Martino, D., 1995, A&A, 303, 127

Forman, W., Jones, C., Cominsky, L., Julien, P., Murray, S., Peters, G., Tananbaum, H., Giacconi, R., 1978, ApJS, 38, 357

Heise, J., Brinkman, A. C., Gronenschild, E., Watson, M. G., King, A. R., Stella, L., Kieboom, K., 1985, A&A, 148, L14

Ishida, M., Silber, A., Bradt, H. V., Remillard, R. A., Makishima, K., Ohashi, T., 1991, ApJ, 367, 270

Kallman, T. R., et al, 1993, ApJ, 411, 869

Kallman, T. R., Mukai, K., Schlegel, E. M., Paerels, F. B., 1996, ApJ, 466, 973

King, A. R., Lasota, J. P., 1979, MNRAS, 188, 653

Kuijpers, J., Pringle, J. E., 1982, A&A, 114, L4

Lamb, D. Q., Masters, A. R., 1979, ApJ, 234, L117

Mason, P., Ramsay, G., Andronov, I., Kolesnikov, S., Shakhovskoy, N., Pavlenko, E., 1998, 295, 511

Mason, K. O., et al 2001, A&A, 365, L36

Nauenberg, M., 1972, ApJ, 175, 417

Piirola, V., Coyne, G. V., Takalo, L., Larsson, S., Vilhu, O., 1994, A&A, 283, 163

Ramsay, G., Mason, K. O., Cropper, M., Watson, M. G., Clayton, K. L., 1994, MNRAS, 270, 692

Ramsay, G., 2000, MNRAS, 314, 403

Ramsay, G., Potter, S., Cropper, M., Buckley, D., Harrop-Allin, M. K., 2000, MNRAS, 316, 225

Schmidt, G., Stockman, H. S., ApJ, 371, 749,

Shrader, C. R., Remillard, R., Silber, A., McClintock, J. E., Lamb, D. Q., 1988, In *A decade of UV astronomy with IUE: Proc. Celebratory Symposium*, ESA SP-281, Vol 1

Silber, A., et al, 1997, MNRAS, 290, 25

Stella, L., Beuermann, K., Patterson, J., 1986, 306, 225

Strüder, L., 2001, 365, L18

Turner, M., et al 2001, A&A, 365, L27

Watson, M. G., King, A. R., Williams, G., 1987, MNRAS, 226, 867